Draft version February 19, 2024
Typeset using LaTeX **manuscript** style in AASTeX631

Two-sided Loop Solar Jet Driven by the Eruption of a Small Filament in a Big Filament Channel

Jiayan Yang,[1] Hechao Chen,[2] Junchao Hong,[1] Bo Yang,[1,3] and Yi Bi[1,3]

[1] *Yunnan Observatory, Chinese Academy of Sciences, P.O. Box 110, Kunming 650011, China*

[2] *School of Physics and Astronomy, Yunnan University, Kunming 650500, China*

[3] *Yunnan Key Laboratory of Solar Physics and Space Science, Kunming 650011, China*

ABSTRACT

Similar to the cases of anemone jets, two-sided loop solar jets could also be produced by either flux emergence from the solar interior or small scale filament eruptions. Using the high-quality data from the *Solar Dynamic Observatory* (*SDO*), we analyzed a two-sided loop solar jet triggered by the eruption of a small filament in this paper. The jet was occurred in a pre-existing big filament channel. The detailed processes involved in the small filament eruption, the interaction between the erupted filament and the big filament channel, and the launch of the two-sided loop jet are presented. The observations further revealed notable asymmetry between the two branches of the jet spire, with the northeastern branch is narrow and short, while the southern branch is wide and long and accompanied by discernible untwisting motions. We explored the unique appearance of the jet by employing the local potential field extrapolation to calculate the coronal magnetic field configuration around the jet. The photospheric magnetic flux below the small filament underwent cancellation for approximately 7 hours before the filament eruption, and the negative flux near the southern foot-point of the filament decreased by about 56 percent during this interval. Therefore, we proposed that the primary photospheric driver of the filament eruption and the associated two-sided loop jet in this event is flux cancellation rather than flux emergence.

Keywords: Solar activity (1475) — Solar filament eruptions (1981) — Solar magnetic fields (1503)

1. INTRODUCTION

Solar jets are ubiquitous transient phenomena occurred in the solar atmosphere. They are collimated plasma beams expelled along open field lines or far-reaching coronal loops, with a width range of $10^2 \sim 10^5$ kilometres (Shimojo & Shibata 2000; Paraschiv et al. 2015). With the aids of advanced ground-based and space-borne solar telescopes, solar jets now could be observed across various wavelengths, from Hα (where they were called as surges; Roy 1973; Jibben & Canfield 2004; Liu 2008; Yang et al. 2012a,b; Li et al. 2017), extreme-ultraviolet (EUV) wavelengths (Nisticò et al. 2009; Chen et al. 2012; Moschou et al. 2013; Zhang et al. 2016), to X-rays (Shibata et al. 1992; Shimojo et al. 1996; Paraschiv et al. 2015). Actually, solar jets are often observed at different wavebands simultaneously (Jiang et al. 2007; Chen et al. 2008; Tang et al. 2021; Yang et al. 2023b).

Morphologically, solar coronal jets are categorized into two types (Shibata et al. 1994a; Shen 2021): straight anemone jets and two-sided loop jets. Anemone jets have been discussed extensively in past decades. Sterling et al. (2015) refer to them as "single-spire jets" since they only exhibit a single spire. The spire of anemone jet often vertical to the solar surface approximately, and a bright point often occurred at the edge of the jet base. In contrast, two-sided loop coronal jets are bidirectional jets. They consist of two roughly antiparallel spires, which usually develop symmetrically from the eruption source region and extend horizontally to the solar surface. The trigger mechanism of both anemone jets and two-sided loop jets is traditionally explained by the emerging-flux model (Shibata et al. 1994a; Yokoyama & Shibata 1995). In this model, a magnetic bi-pole emerging from the solar interior undergoes magnetic reconnection with the ambient pre-existing open field or far-reaching loops, resulting in the formation of jet spires along that open (or far-reaching) field. If the ambient coronal field is oblique or vertical to the solar surface, the produced jet will be an anemone jet; while if the overlying coronal filed is horizontal, a two-sided loop jet will be initiated.

Early magnetohydrodynamic (MHD) simulation of emerging-flux model is 2D (Yokoyama & Shibata 1995). Subsequently, Moreno-Insertis et al. (2008) presented the first 3D numerical experiment of the model, and Moreno-Insertis & Galsgaard (2013) extended the work further. Observations also revealed that some anemone jets were triggered by the emergence of magnetic flux and thus validated the emerging-flux model (Shibata et al. 1994b; Zhang et al. 2000; Chen et al. 2008; Li et al. 2015). Furthermore, Moreno-Insertis & Galsgaard (2013) and some other MHD simulations illuminated that a parasitic bipolar magnetic field emerging from the solar interior would naturally evolve into a sheared arcade. This is consistent with observations that flux emergence is often accompanied by photospheric shear motions, allowing for the transfer of magnetic helicity to the chromosphere and corona (Xu et al. 2022). This sheared arcade would subsequently reconnect with the pre-existed ambient field, and produce a so-called blowout jet (Moore et al. 2010). Therefore, these numerical experiments provided an improved version of the original emerging-flux model. Accordingly, new observations also reported to support the model. Recently, Schmieder et al. (2022) reviewed the research results of surges and jets observed by the Interface Region Imaging Spectrograph (IRIS; De Pontieu et al. 2014). Several cases discussed in their review reported the jets produced by flux emergence, aligning well with the improved emerging-flux model. One of these cases was presented by Ruan et al. (2019). Utilizing IRIS spectrographic observations, they reported bi-directional flows with velocities of nearly ± 200 km s^{-1} in an active region, and attributed these flows to the outflows of magnetic reconnection occurring between emerging flux and a long twisted loop. The magnetic reconnection produced a twisted jet as well. Joshi et al. (2020b) analyzed another twisted jet with the help of IRIS spectrographic observations. They have displayed the detailed process of how the twist transferred from a flux rope located in the reconnection site to the jet. Particularly, Joshi et al. (2020a) studied six recurrent EUV jets observed by SDO/AIA and IRIS simultaneously. They found each of these jets presented a double-chambered structure with cool and hot emissions in each vault, corresponding to the cool and hot loop regions predicted by the emerging-flux models of Moreno-Insertis et al. (2008) and Moreno-Insertis & Galsgaard (2013).

On the other hand, numerous observations have revealed that the generation of anemone jets does not always involve the emergence of magnetic flux, but is closely associated with the eruption of filaments/mini-filaments in the source regions (Hong et al. 2011; Yang et al. 2012a; Sterling et al. 2015; Hong et al. 2016; Shen et al. 2017; Duan et al. 2022). Specifically, jets triggered by mini-filament eruptions typically manifest as blowout jets (Moore et al. 2010), and magnetic flux cancellation rather than flux emergence often occurs before the eruption of mini-filaments and the launch of jets (Adams et al. 2014; Panesar et al. 2016; Joshi et al. 2018; Panesar et al. 2018; Duan et al. 2019; Chen et al. 2020; Yang et al. 2020). Based on the observations of 20 randomly selected solar coronal jets in polar coronal holes, Sterling et al. (2015) found that each of them was driven by the eruption of a mini-filament, and proposed a revised picture to interpret the production of jets. Simulations also support the scenario that filament/mini-filament eruption is the source of coronal jet (Wyper et al. 2017, 2018). Using ultrahigh-resolution 3D magnetohydrodynamic simulations, Wyper et al. (2017) demonstrated the production process of a coronal jet through the eruption of a mini-filament or flux-rope structure embedded in open unipolar field, and its subsequent evolutionary stages. Wyper et al. (2018) further studied in detail three realizations of the model to explain different observational features.

As we mentioned above, theory models for producing solar jets are applicable to both anemone jets and two-sided loop jets. However, comparing with anemone jets, the observational studies of two-sided loop jets are insufficient till now. Some cases have shown magnetic flux emerging from below the photosphere, reconnecting with a pre-existing overlying horizontal field, and producing a two-sided loop jet (Kundu et al. 1998; Jiang et al. 2013; Zheng et al. 2018; Tan et al. 2022), thus supporting the emerging-flux model. Beside these, there are also some other high-resolution observations revealed that the eruption of mini-filaments plays an important role in the formation of two-sided loop jets, aligning with the perspective of Sterling et al. (2015) for anemone jets. Tian et al. (2017) presented observational analysis of two successive two-sided loop jets which were produced not by the emergence of magnetic flux but by the reconnection of two filamentary threads. Sterling et al. (2019) presented an event to show strong evidence that a two-sided loop jet resulted from an erupting

mini-filament, and the magnetic trigger of the eruption is apparently flux cancellation. The examples from Shen et al. (2019) and Yang et al. (2019) further advanced our understanding of two-sided loop jets. Beside confirming the role of mini-filaments in triggering two-sided loop jets, Shen et al. (2019) revealed that the birth of the two-sided loop jet involved two reconnection processes, while Yang et al. (2019) inferred that the mini-filament could reform at the same neutral line after its first eruption and produce recurrent two-sided loop jets. Particularly, Yan et al. (2021) reported that continuous magnetic cancellations could produce a series of unidirectional and bidirectional jets with the eruption of a hot channel rather than a mini-filament.

The current study focuses on a two-sided loop solar jet that appeared in a big filament channel on the eastern part of the solar disk on March 22, 2012. This event provides a good opportunity to investigate the triggering mechanism of two-sided loop solar jets from a perspective of observation, which has been relatively scarce until now. Moreover, this jet deviates from the typical symmetrical spires seen in many two-sided loop jets, exhibiting obvious asymmetric jet spires. Through an examination of the evolution of photospheric magnetic field and the eruption process of the jet, we aimed to identify the trigger of the jet and the reason behind its distinctive appearance. The paper is arranged as follows: the instruments and the data we used are described in Section 2, Section 3 presents the main observational results along with our explanations for the event, and in Section 4 the summary of the event and a brief discussion are given.

2. INSTRUMENTS

The two-sided loop jet we reported in this paper was observed perfectly by the Atmospheric Imaging Assembly (AIA; Lemen et al. 2012) on board the *Solar Dynamics Observatory* (*SDO*; Pesnell et al. 2012). AIA takes full-disk images in 10 UV/EUV passbands with a pixel size of $0''.6$ and a cadence of 12 seconds. We mostly utilize the Level 1.5 images of its 7 EUV passbands here, which are 304 Å (He II, $\log T = 4.7$), 171 Å (Fe IX, $\log T = 5.8$), 193 Å (Fe XII, $\log T = 6.2$), 211 Å (Fe XIV, $\log T = 6.3$), 131 Å (Fe XXI, $\log T = 7.0$), 94 Å (Fe XVIII, $\log T = 6.8$), and 335 Å (Fe XVI, $\log T = 6.4$). The 304 Å and 171 Å images are especially important when analyzing the eruptions of the jet in this event, but the data from other AIA EUV passbands are also examined. Full-disk line-of-sight

(LOS) magnetograms obtained by the Helioseismic and Magnetic Imager (HMI; Scherrer et al. 2012) on board the *SDO* were used to investigate magnetic field in the source region of the jet. These magnetograms were obtained in the Fe I absorption line at 6173 Å with a spatial sampling of $0''.5$ pixel^{-1}, a cadence of 45 seconds, and a noise level of 10 G. All the data are processed by using standard software programs in the SolarSoftWare (*SSW*), and differentially rotated to a reference time close to the event. In addition, to exhibit the site and appearance of the filament channel, we also use Hα line-center images obtained by the Global Oscillation Network Group (GONG; Harvey et al. 1996) at the National Solar Observatory (NSO). The pixel size of the GONG Hα images is $1''$, and the time resolution is 1 minute.

3. OBSERVATIONAL RESULTS

On March 22, 2012, a two-sided loop solar coronal jet was observed by SDO/AIA in the eastern part of the solar disk, near the equator. The jet wasn't associated with any recorded flares or coronal mass ejections (CMEs). Figure 1 displays the location and the general appearance of the jet and its source region. It's worth noting that panel (d) of Figure 1 was captured on February 23, 2012, while other images in this figure were obtained on March 22. As showed by the AIA 171 and 304 Å images (panels (a) and (b)), the jet located at the northeastern end of a large curved dark structure. Upon careful examination of GONG Hα observations, we found that a big quiescent filament (QF) was presented in the same region approximately one solar rotation cycle earlier (panel (d)), and the shape of QF resembles the dark structure seen in panels (a) and (b). However, on the date when the two-sided loop jet occurred, the quiescent filament QF had already disappeared, leaving behind only some fragmented remnants, which are pointed out by the white arrows in the GONG Hα image (panel (c)). Therefore, the dark structure we see in AIA 171 and 304 Å images should be a filament channel (FC). A simultaneous zoomed-in 171 Å image is inserted in panel (a) to provide a clearer view of the jet's appearance. As depicted, the jet consists of a bright jet base and two almost anti-parallel spires. However, unlike typical two-sided loop solar coronal jets, where the two branches of the jet spire are usually symmetrical, the jet presented here exhibits asymmetric branches of the jet spire, i.e., the northeastern spire is short and narrow, while the southern spire is long and wide.

Further examination of the source region of the jet (marked by white boxes in panels (b) and (c)) reveals the presence of a small filament F before the jet occurred (panels (e-g)). In the 04:40:20 UT AIA 304 Å image (panel (f)), F presented itself as a hook-like dark structure, with the length of about $47''.54$ or 3.447×10^4 km. However, it is not easy to identify this small filament in AIA 171 Å and GONG Hα images at the same time. F became more apparent a few minutes later in these wavebands (see panels (e) and (g)), and its shape and the length are differed from what was observed in the 04:40 UT AIA 304 Å image (the outline of F in this image is overlaid as black curves in panels (e) and (g)). By superimposing the contours of an almost simultaneous HMI magnetogram onto the 304 Å image (panel (f)), it was deduced that the northern foot-point of filament F rooted in the positive magnetic field region, while its southern foot-point rooted in the negative region. Additionally, the photospheric magnetic fields beneath F's southern foot-point appeared to be highly sheared. This statement is further supported by the HMI magnetogram superposed with F's outline in panel (h).

Figure 2 presents the eruption process of the small filament F and the following two-sided loop jet. As indicated by the black rectangle in panel (c1), the zoomed-in AIA 304 and 171 Å images of the jet's source region are presented in panels (a1-b4). The filament F is identifiable in these images. It is noticed that, at 04:40:20 UT, a patch of brightening existed beneath the south end of F already (panel (a1)). When tracking AIA and HMI observations before the time, it is inferred that the brightening had been present for about one day since 04:00 UT on March 21, and the photospheric magnetic field in the region has experienced continuous flux cancellations. Therefore, we suppose that the brightening would be a coronal bright point (CBP), which usually appeared in quiet-Sun regions and coronal holes, associated with opposite magnetic polarities in the photosphere, and had an average lifetime of about 28 hours in EUV images (Hong et al. 2014). However, the CBP did not contain any filament until 04:00 UT on March 22. In the accompanying animation of Figure 2 which starts at 04:00 UT on March 22, it is noticed that F was unrecognizable at the very beginning, and then it started to form a few minutes later. Consistent with panel (a1), at 04:40 UT F could be identified clearly at the animation. Therefore, although AIA images did not got sufficient resolution

to reveal either the exact time or the detailed process of F's formation, we could infer that F formed between 04:00 UT and 04:40 UT on March 22.

The new-formed small filament F was obvious and stable at 04:40:20 UT as showed in the AIA 304 Å image (panel (a1)), but it soon started to lift soon. When superimposing the original position of F (blue curves, obtained from panel (a1)) to other 304 Å images in the top row, it is clear that F erupted southeastwardly, approaching the big filament channel FC. The CBP also became brighter and more expanded, evolved into a small flare eventually. The subsequent movement of the erupting filament is more clearly visible in AIA 171 Å images (panels (b1)-(b4)). As pointed out by the white arrows in panels (b1) and (b2), F erupted towards the pre-existing filament channel FC, and its appearance changed a lot compared to the original form in AIA 304 Å image (blue curve). The overlying magnetic field of erupting F would reconnect with the magnetic field of FC, resulting in the launch of a jet. Dark filament plasma was observed to be ejected into FC, and some brightenings occurred at the interface of them, which were likely signatures of the magnetic reconnection (panels (b3) and (b4)). Then, bright mass flow streamed from a bright point near the flare and flowed southwardly into FC.

The observed bright mass flow indicates the initiation of the jet, while the complete appearance and development of the jet were displayed in panels (c1)-(c4) of AIA 171 Å images with a larger field of view (FOV) . In these pictures, it is evident that the bright jet plasma flowed both southwardly and northeasterly, forming two roughly antiparallel jet spires, and the small flare associated with the filament eruption evolved into the jet bright point (JBP). Based on the appearance of the jet and the trajectory of F's eruption, it can be deduce that the jet was a two-sided loop solar jet triggered by the eruption of the small filament F. Therefore, this event supports the picture proposed by Sterling et al. (2015), confirms once again that two-sided loop solar jets could also be produced by the eruption of small scale filaments. It is consistent with recent observations of two-sided loop jets (Shen et al. 2019; Sterling et al. 2019; Yang et al. 2019). It is obvious that the northeastern spire of the jet is short and narrow, resembling a standard jet, while the southern spire is long and wide, resembling a blowout jet (Moore et al. 2010). In this sense, the jet is particular, since most two-sided loop jets

typically have roughly symmetrical spires (Jiang et al. 2013; Sterling et al. 2019; Yang et al. 2019). Additionally, the northeastern spire of the jet appears bright, indicating it is composed mainly of hot plasma, while the southern spire is a mixture of cold and hot mass, and exhibits noticeable untwisting motion (see the accompanying animation).

Panel (d) of Figure 2 displays the normalized AIA 304 and 171 Å light curves measured in the white boxes in panels (a4), (b3), and (c4). The light curves show the evolution of the intensity of the CBP (or the flare, or JBP). It is noticed that the brightness of the patch began to increase sharply at around 04:45 UT, indicating the beginning of F's eruption. Both the 304 and 171 Å light curves reached their first peak simultaneously at approximately 04:49 UT, as indicated by the vertical dotted line. This peak should correspond to the maximum intensity of the small flare produced by the filament eruption. Subsequently, the intensities of the 304 and 171 Å images in the region decreased for a while, then increased again and reached the their maximum value. This second stage of increasing of intensity may indicate the launch of the jet, and the maximum of the light curve corresponds to the maxima of the JBP caused by the jet. Note that the time of maximum intensity differs when measured in different wavebands: the 171 Å light curve reached its peak at about 05:11 UT, as indicated by the vertical dashed line, while the 304 Å light curve reached its peak at about 05:07 UT, a few minutes before the maximum of the 171 Å light curve.

To analyze the evolution of the jet in detail, time-slice plots were constructed from AIA 304, 171, and 131 Å images and displayed in Figure 3. In this figure, panels (a)-(c) show the time-slices constructed along slit S1, while panel (d) presents the time-slice along slit S2. Slit S1 is a curved line segment along the jet spire, pointing from the northeast to the south, as shown by the white arrows in panels (c3) and (c4) of Figure 2. Slit S2, on the other hand, is a straight line segment roughly vertical to the southern branch of the jet spire. In panel (b) of Figure 3, the horizontal dashed line represents the locations of the demarcation point of the jet spire at different times, corresponding to the blue asterisks in Figure 2. Therefore, in this image, the region above the dashed line describes the southward ejection of the jet, while the region below the line shows the northeastern ejection of the jet. The ejections along the two branches of the jet spire show notable differences. The southward

ejections are generally more vigorous, with a larger amount of plasma being ejected. Furthermore, the southward ejections are steady and continuous, consisting of both dark and bright components, indicating the ejection of cold filament mass into the southern branch of the jet spire. All three time-slices along S1 (panels (a-c)) show that the mass ejection along the southern branch of the jet spire can be divided into two stages: a slow ejection stage with an average projected speed of about 18.09 km s^{-1}, as measured in 171 Å time-slice, and a fast ejection stage with an average projected speed of about 165.05 km s^{-1}. This behavior is similar to the eruption of a filament, which aligns with what we inferred from Figure 2 that the jet was triggered by a small filament eruption. Zhang et al. (2021) also found that the kinetic evolution of an anemone jet triggered by a mini-filament eruption can be divided into a slow rise phase and a fast rise phase, and they suggested that these two phases may correspond to the magnetic reconnections at the breakout current sheet and the flare current sheet, respectively. According to the 304 Å time-slice (panel (a)), the fast ejection of the jet started at about 05:00:29 UT, as indicated by the vertical dashed lines in the figure. On the other hand, the northeastern ejections are intermittent and primarily consist of the bright component. Three episodes of intermittent northeastern mass ejection are marked by red dotted lines in panel (b), with measured average speeds of 179.32 km s^{-1}, 97.53 km s^{-1}, and 171.52 km s^{-1}, respectively. Indeed, the speeds of the intermittent northeastern ejections are roughly comparable to the fast ejection of the southern branch. However, the two-stages mass ejection was indistinguishable in the northeastern branch of the jet spire, possibly because the ejection was weak there. From the time-slice plots, the presence of the cold filament mass in the northeastern ejections may not be apparent, but the accompanying AIA 171 Å animation shown in Figure 2 reveals that, although the majority of F's mass was ejected into the southern branch of the jet spire, a small portion of the dark filament mass was also ejected into the northeastern spire of the jet.

AIA animation accompanying Figure 2 showed that the southern branch of the jet spire underwent a significant untwisting motion. This character was even more apparent in the time-slice plot along slit S2 (panel (d)). From the time-slice, it was evident that some complicated transverse motions took place in the jet's southern spire soon after the fast ejection of the jet. However, the width

of the jet spire did not show a significant change, suggesting that the jet spire experienced only rotational motion without expansion. Untwisting motion is a common character in blowout jets (Hong et al. 2013; Moore et al. 2015; Li & Yang 2019; Chen et al. 2021), and it has been explained as the release of the twist initially stored in the twisted filament's magnetic field through magnetic reconnection with the ambient coronal magnetic field. Two episodes of the untwisting motion were traced by the dotted white lines in panel (d), with linear fitting velocities of 295.37 km s^{-1} and 211.46 km s^{-1}. These rotational velocities were relatively large compared to many previous studies (Zhang & Ji 2014; Moore et al. 2015; Yang et al. 2023b), but still within a reasonable range. The time-slice further showed that the rotational direction of the southern spire of the jet was along the forward direction of S2, from the east to the west, according to the white arrow in panel (c4) of Figure 2. This direction is consistent with what we see in the AIA 171 Å animation. Therefore, the southern spire of the jet experienced an anticlockwise rotation when viewed from JBP.

Figure 4 and its accompanying animation displayed the situation of the photospheric magnetic field before and during the eruptions of the filament F and the following two-sided loop jet. It is revealed that, in the source region of the jet (as indicated by the black circles in the top half part of Figure 4), the positive and negative photospheric magnetic polarities moved toward and canceled to each other since 21:30 UT on March 21. After 01:00 UT on March 22, the cancellation occurred mainly in the region indicated by the white ovals in the figure and the animation. When superposing the outline of the small filament F obtained from the 04:40 UT AIA 304 Å image onto the simultaneous magnetogram showed in panel (a8), it is clear that the region in the white oval is where F's southern foot-point rooted. HMI LOS magnetograms revealed that the negative polarity patch of the photospheric magnetic field (the black patch) continuously moved to northwestward, while the positive polarity patch (the white patch) moved southeastward. After several hours of movement and cancelation, the photospheric magnetic field below F's southern foot-point became highly sheared (panel (a8)), causing the southern part of the filament to raise first, followed by the entire filament's eruption.

To demonstrate the magnetic flux cancellation in the source region of the jet more intuitively, we present the change of the unsigned positive (red curves) and negative (black curves) magnetic fluxes in panels (b) and (c) respectively. In panel (b), the flux curves are calculated within the region indicated by the black circles, while in panel (c), the flux curves are calculated within the region indicated by the white ovals. It is showed that, the negative magnetic fluxes in both regions exhibit a nearly monotonic decrease, with the exception of a short period from 00:00 UT to 01:00 UT when a small patch of negative polarity moved into the black circle region from the south, as shown in the accompanying animation. From 21:45 UT of the previous day to 04:45 UT of March 22, the negative magnetic fluxes around F's southern foot-point decreased for about 7 hours before its eruption (indicated by the blue vertical lines), suggesting that the magnetic flux cancellation occurred for several hours prior to the eruption. On the other hand, the positive magnetic flux only showed a slight decrement from 23:00 UT on March 21 to 01:00 UT on March 22, and changed little during other measured periods. Checking the HMI animation carefully, we realize that isolating the positive magnetic field into these regions is more difficult compare to the negative field because its dispersed nature. Convergence motion frequently brought some positive magnetic polarities moved into the regions, thereby enhancing the calculated positive fluxes. Additionally, it appears that some positive polarities emerged in the regions during the flux measurements, further enhancing the positive fluxes. However, even with the inclusion of these extra fluxes, the positive fluxes shown in panels (b) and (c) do not increase significantly, implying cancellation with the negative fluxes at their interface.Therefore, we suspect that the eruptions of the small filament F and the subsequent two-sided loop jet in this event are driven by photospheric magnetic flux cancellation, similar to cases of many anemone jets (Hong et al. 2011; Panesar et al. 2016, 2018) and two-sided loop jets (Sterling et al. 2019; Yang et al. 2019) driven by mini-filament eruptions. The negative flux in the black circle region decreased from 2.7×10^{19} Mx to 1.2×10^{19} Mx within 7 hours, thus the flux reduction is about 56%, and the cancelation rate is about 2.1×10^{18} Mx hr^{-1}. The values of the negative fluxes in the white oval regions are smaller due to the smaller region size, but the flux reduction and cancelation rate are approximately the same as those in the black circle region.

According to previous observations, anemone jets are usually observed to be vertical to the solar surface, while two-sided loop jets are typically parallel to the solar surface, with two symmetrical branches of jet spire. The two-sided loop jet we reported here was nearly parallel to the solar surface since it occurred in a filament channel, but exhibited a distinctive appearance of asymmetrical branches of the jet spire. To interpret the asymmetry of the two branches of the jet spire, we investigated the topology of the coronal magnetic field around the jet. Since we lacked vector magnetic field data as the jet took place in the quiescent region of the solar disk, we employed the local potential field extrapolation method (Alissandrakis 1981; Gary 1989) to calculate the coronal magnetic field configuration prior to the filament eruption, which is presented in Figure 5. In panel (a) which is the front view of the solar disk, we adopted an AIA 171 Å image near the maximum of the jet spire as the background image, and superimposed extrapolated coronal field lines before the filament eruption at four representative positions above the jet's spire. The coronal magnetic field lines above the northeastern branch of the jet's spire are denoted by the cyan and yellow curves, while the coronal magnetic field lines above the southern branch of the jet's spire are denoted by the green and white curves. In panel (b) which is the same image from a sideways perspective, the colors of the field lines match those in panel (a). Combining these two panels, it is evident that the magnetic arches above the southern branch of the jet's spire have large heights and spans, even far away from JBP (see the white curves). Therefore, this coronal magnetic configuration provides abundant space for the southern spire to extend. In contrast, the situation is different for the northeastern branch of the jet's spire. The heights and spans of the magnetic arches above the northeastern spire are relatively small compared to those above the southern spire (see the yellow curves), thus the coronal magnetic field confines the jet spire to a narrow flow. Furthermore, the coronal magnetic field becomes vertical not far ahead of the northeastern spire (see the cyan curves), cutting off the jet spire. Therefore, the northeastern branch of the jet's spire is narrow and short. Considering that the two-sided loop jet occurred in a big filament channel near its northeast end, the extrapolated coronal magnetic configuration around the jet and the asymmetrical appearance of the jet's spire are reasonable.

4. SUMMARY AND DISCUSSION

Using the perfect observations from *SDO*/AIA and HMI, this paper presents an analysis of a two-sided loop solar coronal jet. The jet occurred in a large filament channel located in the southeast part of the solar disk. AIA observations revealed that a pre-existing small filament erupted in the source region just a few minutes before the jet occurred, and captured the detailed processes of how the erupted small filament ejected into the adjacent filament channel and triggered the two-sided loop jet. The observations confirmed that, besides the widely accepted emerging-flux model (Shibata et al. 1994a; Yokoyama & Shibata 1995), two-sided loop solar jets can also be produced by the magnetic reconnection between the overlying magnetic field of an erupting small filament and the ambient coronal magnetic field, just like in the cases of anemone jets (Sterling et al. 2015; Hong et al. 2016; Li et al. 2017; Yang et al. 2023a). The observations further showed that two branches of the jet's spire are heavily asymmetrical, with the southern branch being wide and long while the northeastern branch is narrow and short. By investigating the coronal magnetic configuration around the jet, we suspect that this unique appearance is due to the asymmetric coronal magnetic configuration near the end of the filament channel.

The trigger mechanism of solar coronal jets is an important issue for the studies of both anemone jets and two-sided loop jets. While the event presented here maintains the picture of Sterling et al. (2015), in general, either the emerging-flux model (Shibata et al. 1994a; Yokoyama & Shibata 1995; Moreno-Insertis et al. 2008; Moreno-Insertis & Galsgaard 2013) or the mini-filament-eruption-driven picture (Sterling et al. 2015; Wyper et al. 2017, 2018) has been supported by many observation cases respectively, and the structures and kinematic characteristics of jets produced by these two mechanisms did not show much difference from one to the other (Schmieder et al. 2022; Shen 2021). Therefore, it seems that in a pre-existing background field, both the direct emergence of magnetic flux from the interior and the eruption of filament/mini-filament could effectively trigger reconnection between two magnetic systems and produce a solar jet.

For the jets that conform to the emerging-flux model, flux emergence is always observed and regarded as a key driver in photosphere (Shibata et al. 1994b; Zhang et al. 2000; Chen et al. 2008; Li et al. 2015). However, in the cases that jets are driven by erupting mini-filaments, flux cancella-

tion is typically predominant rather than flux emergence (Sterling et al. 2015; Panesar et al. 2016; Sterling et al. 2019; Yang et al. 2019, 2023a). In some cases, it seems that both flux emergence and cancellation worked together (Jiang et al. 2007; Shen et al. 2017, 2019). In our event, the positive magnetic flux in the source region of the jet did not change much, but the negative flux decreased monotonously for about 7 hours before the eruptions of the small filament and the following two-sided loop jet. Therefore, although could not exclude the contribution of flux emergence completely, we still propose that the main photospheric driver of this two-sided loop jet is flux cancellation, consistent with previous studies on jets triggered by mini-filament eruptions. A study by Panesar et al. (2016) of 10 random solar jets in quiescent regions found that each one experienced flux reduction between 21% and 57% at the neutral line below a mini-filament. In another investigation of 13 random solar jets in coronal holes, the authors found that the flux reduction ranged from 21% to 73%, with a calculated average cancellation rate of 0.6×10^{18} Mx hr^{-1} (Panesar et al. 2018). The value of average cancellation rate is 1.5×10^{18} Mx hr^{-1} for the quiescent region jets they studied previously (Panesar et al. 2016). In comparison, the active region jets studied by Sterling et al. (2017) had an average cancellation rate of 15×10^{18} Mx hr^{-1}. The two-sided loop jet in our event occurred in a quiescent region, with magnetic flux reduction of 56% and an average cancellation rate of 2.1×10^{18} Mx hr^{-1}. Therefore, it seems that the flux cancellation in this event was a little more violent than the quiescent region jets studied by Panesar et al. (2016), but was still within a reasonable range. This may be due to the small filament in this event being slightly larger than the mini-filaments in their events, thus more free magnetic energy are required to trigger the eruption of the filament.

Similar to filaments eruption of ordinary scale, the eruption of small scale filaments and the following coronal jets occasionally result in flares and narrow CMEs (Yang et al. 2020). The jets can also interact with other magnetic structures during their ejections. More recently, Joshi et al. (2023) reported two observational events of large-amplitude filament oscillations triggered by solar coronal jets. In both events, a jet formed near one end of a large filament due to flux emergence. The ejected jet hit the filament channel from the end, leading to large-amplitude oscillation in the filament, which supported the MHD numerical experiments recently conducted by Luna & Moreno-Insertis (2021).

In the present event, the jet also occurred near the end of a large filament channel. However, during the jet's ejection, the filament channel contained little filament plasma, as indicated by the GONG Hα image in Figure 1. Therefore, the interaction between the jet and the filament channel was not observed in this event.

In summary, this paper presents the observations of a two-sided loop solar jet in a large filament channel with asymmetrical spires. The jet was triggered by the eruption of a small filament, and the main driver of the filament eruption and the jet was the continuous cancellation of positive and negative magnetic fluxes in the photosphere. Compared with anemone jets, there is still limited research on two-sided loop jets, and more observations with high spatial and temporal resolution are needed in the future to further understand their characteristics and underlying mechanisms.

We thank an anonymous referee for many constructive suggestions and thoughtful comments that improved the quality of this paper. The authors thank the *SDO* and GONG teams for granting free access to their internet databases. This work is supported by the B-type Strategic Priority Program No. XDB41000000 and XDB0560000 funded by the Chinese Academy of Sciences, the National Key R&D Program of China (2019YFA0405000), the National Natural Science Foundation of China under grants 12273108, 11933009, 12173084, 12073072, and 12273106, and by the "Yunnan Revitalization Talent Support Program" Innovation Team Project.

REFERENCES

Adams, M., Sterling, A. C., Moore, R. L., & Gary, G. A. 2014, ApJ, 783, 11, doi: 10.1088/0004-637X/783/1/11

Alissandrakis, C. E. 1981, A&A, 100, 197

Chen, H., Hong, J., Yang, B., Xu, Z., & Yang, J. 2020, ApJ, 902, 8, doi: 10.3847/1538-4357/abb1c1

Chen, H., Yang, J., Hong, J., Li, H., & Duan, Y. 2021, ApJ, 911, 33, doi: 10.3847/1538-4357/abe6a8

Chen, H. D., Jiang, Y. C., & Ma, S. L. 2008, A&A, 478, 907, doi: 10.1051/0004-6361:20078641

Chen, H.-D., Zhang, J., & Ma, S.-L. 2012, Research in Astronomy and Astrophysics, 12, 573, doi: 10.1088/1674-4527/12/5/009

De Pontieu, B., Title, A. M., Lemen, J. R., et al. 2014, SoPh, 289, 2733, doi: 10.1007/s11207-014-0485-y

Duan, Y., Shen, Y., Chen, H., & Liang, H. 2019, ApJ, 881, 132, doi: 10.3847/1538-4357/ab32e9

Duan, Y., Shen, Y., Zhou, X., et al. 2022, ApJL, 926, L39, doi: 10.3847/2041-8213/ac4df2

Gary, G. A. 1989, ApJS, 69, 323, doi: 10.1086/191316

Harvey, J. W., Hill, F., Hubbard, R. P., et al. 1996, Science, 272, 1284, doi: 10.1126/science.272.5266.1284

Hong, J., Jiang, Y., Yang, J., et al. 2014, ApJ, 796, 73, doi: 10.1088/0004-637X/796/2/73

—. 2016, ApJ, 830, 60, doi: 10.3847/0004-637X/830/2/60

Hong, J., Jiang, Y., Zheng, R., et al. 2011, ApJL, 738, L20, doi: 10.1088/2041-8205/738/2/L20

Hong, J.-C., Jiang, Y.-C., Yang, J.-Y., et al. 2013, Research in Astronomy and Astrophysics, 13, 253, doi: 10.1088/1674-4527/13/3/001

Jiang, Y., Bi, Y., Yang, J., et al. 2013, ApJ, 775, 132, doi: 10.1088/0004-637X/775/2/132

Jiang, Y. C., Chen, H. D., Li, K. J., Shen, Y. D., & Yang, L. H. 2007, A&A, 469, 331, doi: 10.1051/0004-6361:20053954

Jibben, P., & Canfield, R. C. 2004, ApJ, 610, 1129, doi: 10.1086/421727

Joshi, N. C., Nishizuka, N., Filippov, B., Magara, T., & Tlatov, A. G. 2018, MNRAS, 476, 1286, doi: 10.1093/mnras/sty322

Joshi, R., Chandra, R., Schmieder, B., et al. 2020a, A&A, 639, A22, doi: 10.1051/0004-6361/202037806

Joshi, R., Luna, M., Schmieder, B., Moreno-Insertis, F., & Chandra, R. 2023, A&A, 672, A15, doi: 10.1051/0004-6361/202245647

Joshi, R., Schmieder, B., Aulanier, G., Bommier, V., & Chandra, R. 2020b, A&A, 642, A169, doi: 10.1051/0004-6361/202038562

Kundu, M. R., Raulin, J. P., Nitta, N., Shibata, K., & Shimojo, M. 1998, SoPh, 178, 173, doi: 10.1023/A:1005018109815

Lemen, J. R., Title, A. M., Akin, D. J., et al. 2012, SoPh, 275, 17, doi: 10.1007/s11207-011-9776-8

Li, H., & Yang, J. 2019, ApJ, 872, 87, doi: 10.3847/1538-4357/aafb3a

Li, H., Jiang, Y., Yang, J., et al. 2017, ApJL, 842, L20, doi: 10.3847/2041-8213/aa762c

Li, H. D., Jiang, Y. C., Yang, J. Y., Bi, Y., & Liang, H. F. 2015, Ap&SS, 359, 4, doi: 10.1007/s10509-015-2490-5

Liu, Y. 2008, SoPh, 249, 75, doi: 10.1007/s11207-008-9176-x

Luna, M., & Moreno-Insertis, F. 2021, ApJ, 912, 75, doi: 10.3847/1538-4357/abec46

Moore, R. L., Cirtain, J. W., Sterling, A. C., & Falconer, D. A. 2010, ApJ, 720, 757, doi: 10.1088/0004-637X/720/1/757

Moore, R. L., Sterling, A. C., & Falconer, D. A. 2015, ApJ, 806, 11, doi: 10.1088/0004-637X/806/1/11

Moreno-Insertis, F., & Galsgaard, K. 2013, ApJ, 771, 20, doi: 10.1088/0004-637X/771/1/20

Moreno-Insertis, F., Galsgaard, K., & Ugarte-Urra, I. 2008, ApJL, 673, L211, doi: 10.1086/527560

Moschou, S. P., Tsinganos, K., Vourlidas, A., & Archontis, V. 2013, SoPh, 284, 427, doi: 10.1007/s11207-012-0190-7

Nisticò, G., Bothmer, V., Patsourakos, S., & Zimbardo, G. 2009, SoPh, 259, 87, doi: 10.1007/s11207-009-9424-8

Panesar, N. K., Sterling, A. C., & Moore, R. L. 2018, ApJ, 853, 189, doi: 10.3847/1538-4357/aaa3e9

Panesar, N. K., Sterling, A. C., Moore, R. L., & Chakrapani, P. 2016, ApJL, 832, L7, doi: 10.3847/2041-8205/832/1/L7

Paraschiv, A. R., Bemporad, A., & Sterling, A. C. 2015, A&A, 579, A96, doi: 10.1051/0004-6361/201525671

Pesnell, W. D., Thompson, B. J., & Chamberlin, P. C. 2012, SoPh, 275, 3, doi: 10.1007/s11207-011-9841-3

Roy, J. R. 1973, SoPh, 32, 139, doi: 10.1007/BF00152734

Ruan, G., Schmieder, B., Masson, S., et al. 2019, ApJ, 883, 52, doi: 10.3847/1538-4357/ab3657

Scherrer, P. H., Schou, J., Bush, R. I., et al. 2012, SoPh, 275, 207, doi: 10.1007/s11207-011-9834-2

Schmieder, B., Joshi, R., & Chandra, R. 2022, Advances in Space Research, 70, 1580, doi: 10.1016/j.asr.2021.12.013

Shen, Y. 2021, Proceedings of the Royal Society of London Series A, 477, 217, doi: 10.1098/rspa.2020.0217

Shen, Y., Liu, Y. D., Su, J., Qu, Z., & Tian, Z. 2017, ApJ, 851, 67, doi: 10.3847/1538-4357/aa9a48

Shen, Y., Qu, Z., Yuan, D., et al. 2019, ApJ, 883, 104, doi: 10.3847/1538-4357/ab3a4d

Shibata, K., Nitta, N., Matsumoto, R., et al. 1994a, in X-ray solar physics from Yohkoh, ed. Y. Uchida, T. Watanabe, K. Shibata, & H. S. Hudson, 29

Shibata, K., Nitta, N., Strong, K. T., et al. 1994b, ApJL, 431, L51, doi: 10.1086/187470

Shibata, K., Ishido, Y., Acton, L. W., et al. 1992, PASJ, 44, L173

Shimojo, M., Hashimoto, S., Shibata, K., et al. 1996, PASJ, 48, 123, doi: 10.1093/pasj/48.1.123

Shimojo, M., & Shibata, K. 2000, ApJ, 542, 1100, doi: 10.1086/317024

Sterling, A. C., Harra, L. K., Moore, R. L., & Falconer, D. A. 2019, ApJ, 871, 220, doi: 10.3847/1538-4357/aaf1d3

Sterling, A. C., Moore, R. L., Falconer, D. A., & Adams, M. 2015, Nature, 523, 437, doi: 10.1038/nature14556

Sterling, A. C., Moore, R. L., Falconer, D. A., Panesar, N. K., & Martinez, F. 2017, ApJ, 844, 28, doi: 10.3847/1538-4357/aa7945

Tan, S., Shen, Y., Zhou, X., et al. 2022, MNRAS, 516, L12, doi: 10.1093/mnrasl/slac069

Tang, Z., Shen, Y., Zhou, X., et al. 2021, ApJL, 912, L15, doi: 10.3847/2041-8213/abf73a

Tian, Z., Liu, Y., Shen, Y., et al. 2017, ApJ, 845, 94, doi: 10.3847/1538-4357/aa8095

Wyper, P. F., Antiochos, S. K., & DeVore, C. R. 2017, Nature, 544, 452, doi: 10.1038/nature22050

Wyper, P. F., DeVore, C. R., & Antiochos, S. K. 2018, ApJ, 852, 98, doi: 10.3847/1538-4357/aa9ffc

Xu, Z., Yan, X., Yang, L., et al. 2022, ApJL, 937, L11, doi: 10.3847/2041-8213/ac8fef

Yan, X., Wang, J., Guo, Q., et al. 2021, ApJ, 919, 34, doi: 10.3847/1538-4357/ac116d

Yang, B., Yang, J., Bi, Y., et al. 2019, ApJ, 887, 220, doi: 10.3847/1538-4357/ab557e

Yang, J., Hong, J., Li, H., & Jiang, Y. 2020, ApJ, 900, 158, doi: 10.3847/1538-4357/aba7c0

Yang, J., Hong, J., Yang, B., Bi, Y., & Xu, Z. 2023a, ApJ, 942, 86, doi: 10.3847/1538-4357/aca66f

Yang, J., Jiang, Y., Yang, B., et al. 2012a, NewA, 17, 732, doi: 10.1016/j.newast.2012.05.006

Yang, J.-Y., Jiang, Y.-C., Yang, D., et al. 2012b, Research in Astronomy and Astrophysics, 12, 300, doi: 10.1088/1674-4527/12/3/006

Yang, L., Yan, X., Xue, Z., et al. 2023b, ApJ, 945, 96, doi: 10.3847/1538-4357/acb6f6

Yokoyama, T., & Shibata, K. 1995, Nature, 375, 42, doi: 10.1038/375042a0

Zhang, J., Wang, J., & Liu, Y. 2000, A&A, 361, 759

Zhang, Q. M., Huang, Z. H., Hou, Y. J., et al. 2021, A&A, 647, A113, doi: 10.1051/0004-6361/202038924

Zhang, Q. M., & Ji, H. S. 2014, A&A, 561, A134, doi: 10.1051/0004-6361/201322616

Zhang, Q. M., Ji, H. S., & Su, Y. N. 2016, SoPh, 291, 859, doi: 10.1007/s11207-016-0878-1

Zheng, R., Chen, Y., Huang, Z., et al. 2018, ApJ, 861, 108, doi: 10.3847/1538-4357/aac955

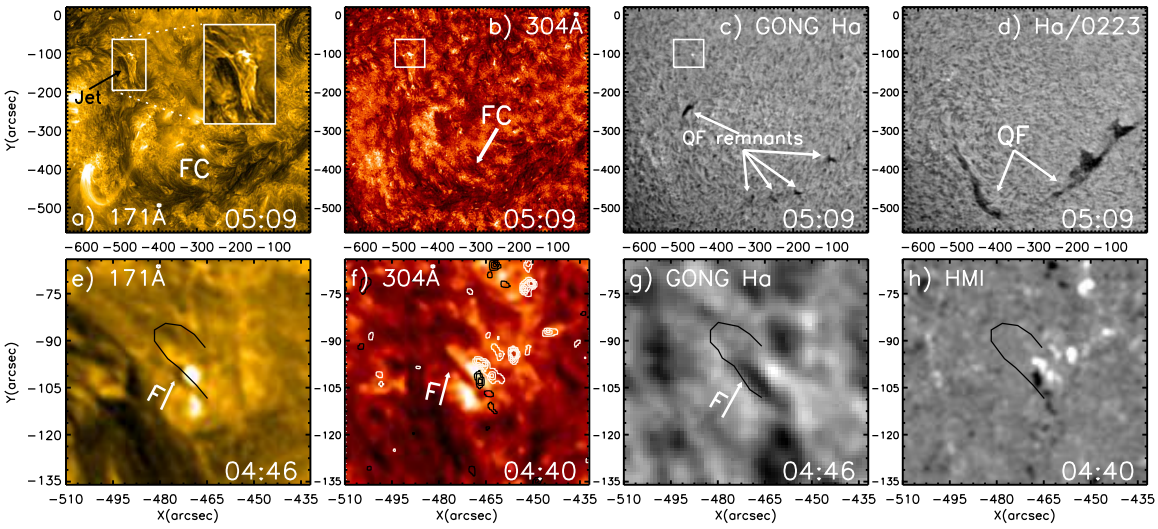

Figure 1. General appearance of the two-sided loop solar jet and its circumstances (top row) and its source region (bottom row) showed by AIA 171 Å, 304 Å, GONG Hα line-center images, and HMI LOS magnetogram. The field of view (FOV) of the top row is $635'' \times 585''$, while the FOV of the bottom row is $78'' \times 72''$, which is indicated by the white boxes in panels (b) and (c). A zoomed-in image of the two-sided loop jet is inserted in panel (a) to highlight it more clearly. The outline of the axis of the small filament F obtained from panel (f) is overlaid as black curves in the other panels of the bottom row. The LOS magnetic field measured in the 04:40:16 UT HMI magnetogram are superimposed on the AIA 304 Å image (panel (f)) as black and white contours, with the intensity of ± 20, ± 40, ± 60, ± 80, and ± 100 Gauss.

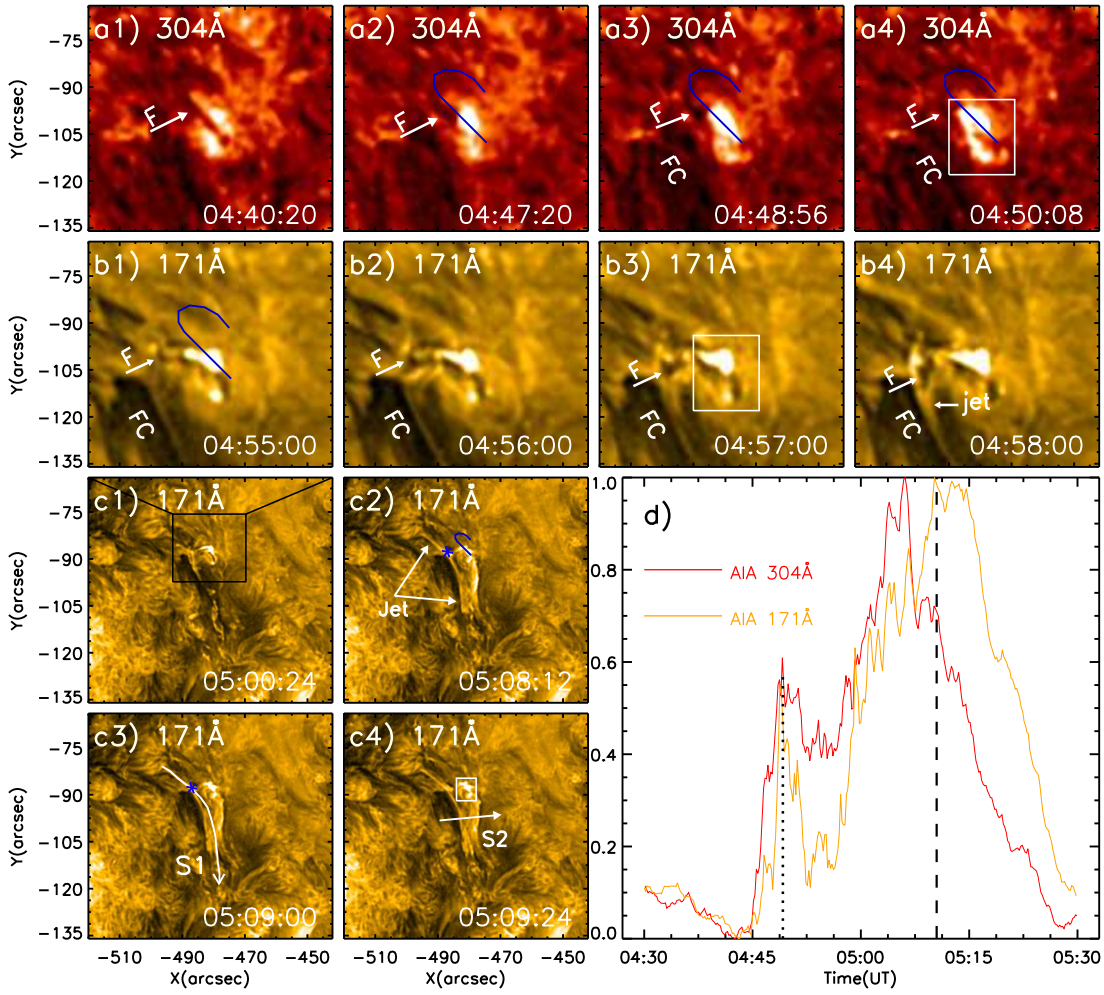

Figure 2. AIA 304 and 171 Å images illustrate the eruption of the filament F (panels (a1)-(b4)) and the associated two-sided loop jet (panels (c1)-(c4)). Some panels are overlaid with the outline of F's axis obtain from the 04:40:20 UT 304 Å image as blue curves. The long curved white arrow in panel (c3) and the white arrow in panel (c4) indicate the slit positions of the time slices shown in Figure 3, while the blue asterisks in panels (c2) and (c3) show the approximate position of the demarcation point of the jet's spires. The black rectangle in panel (c1) indicates the FOV of panels (a1)-(b4), which is $78'' \times 72''$, the same as the bottom row of Figures 1. The FOV of panels (c1)-(c4) is $260'' \times 240''$. Panel (d) presents the normalized light curves of AIA 304 and 171 Å intensities in the region indicated by the white boxes in panels (a4), (b3), and (c4). (An animation of AIA 171, 193, 304 Å direct images and GONG Hα line-center images is available. The animation lasts 15 seconds, has the same FOV as panels (c1)-(c4), and covers the time from 04:00 UT to 05:29 UT. The cadence of the AIA images is 12s, while the cadence of the GONG images is 1m.)

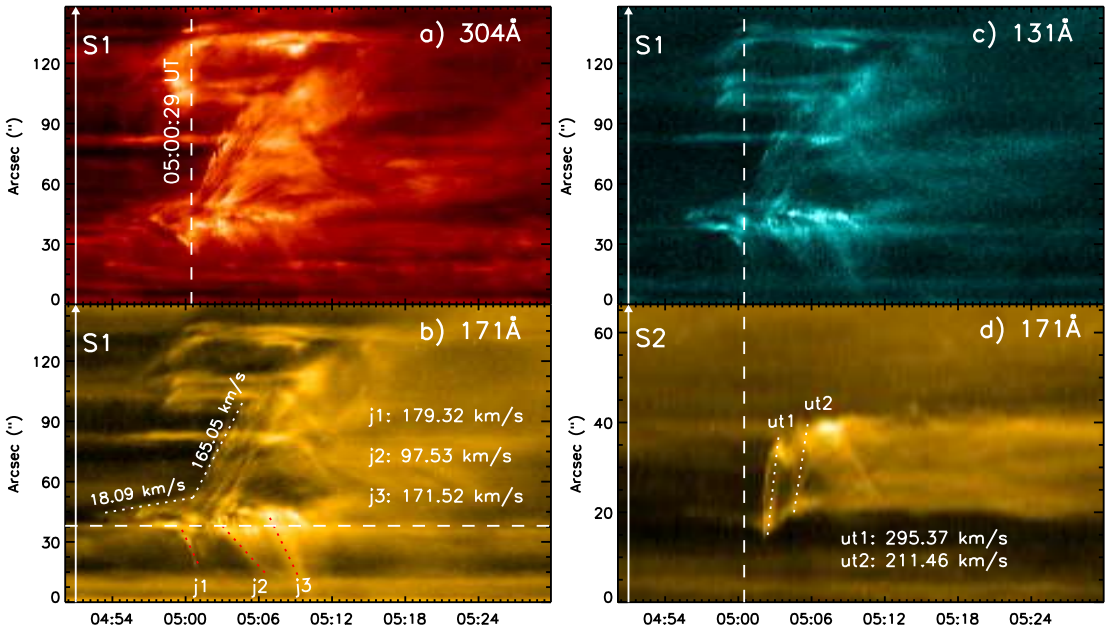

Figure 3. The time-space plots in AIA 304, 171, and 131 Å wavebands. Panels (a)-(c) present the time-slices along slit S1, while panel (d) presents the time-slice along slit S2. The positions of these slits are showed in Figure 2c. The vertical dashed lines indicate the start time of the jet, while the horizontal dashed line denotes the position of the demarcation point of the jet's spire. The dotted lines in panels (b) and (d) track the mass ejections in both branches of the jet spire and the transverse motion in the southern branch, respectively, with the measured projected velocities presented also.

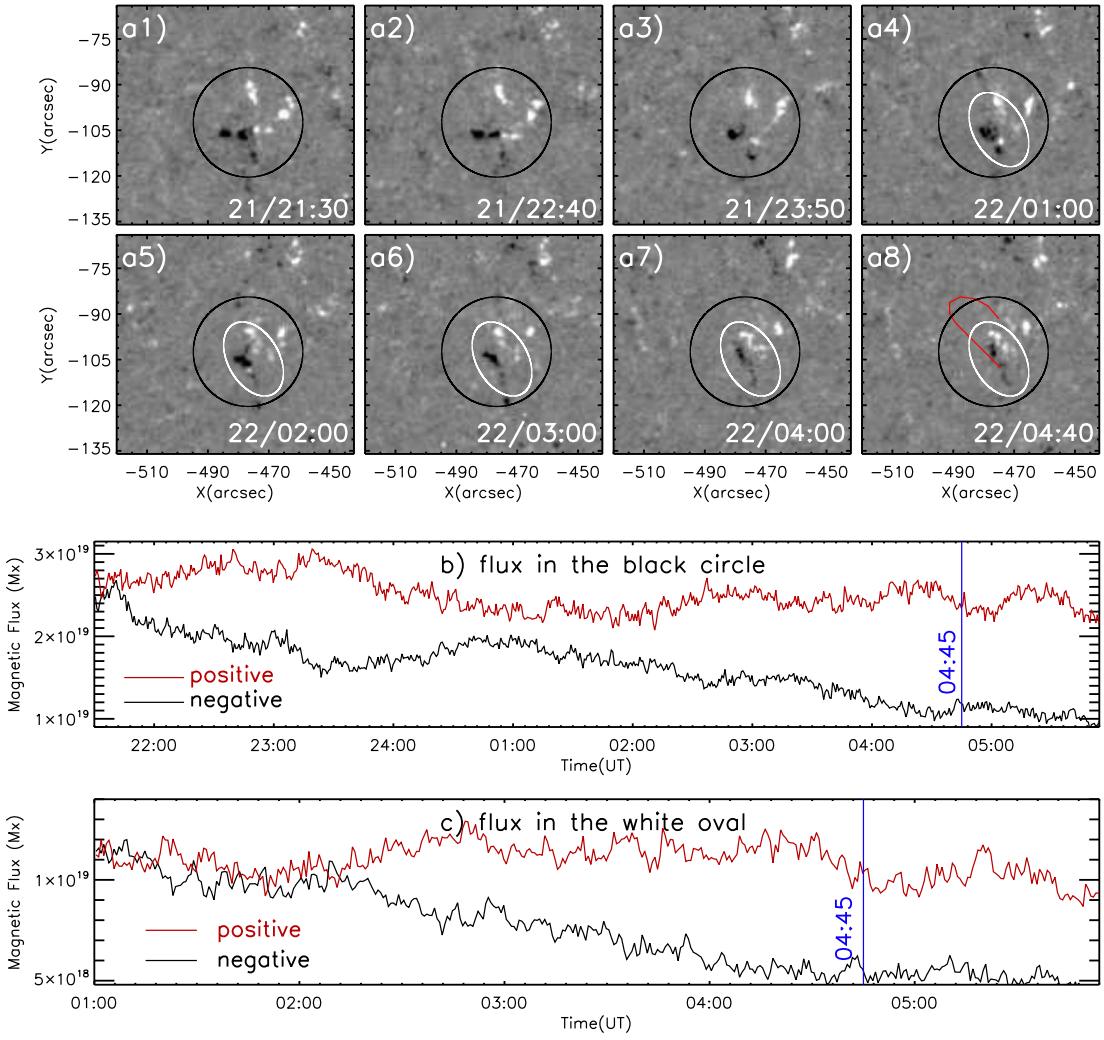

Figure 4. Evolution of the photospheric magnetic field in the source region of the two-sided loop jet. (a1-a8) HMI LOS magnetograms show the cancellation between the positive and negative magnetic polarities. The red curve in panel (a8) represents the outline of F's axis obtained from the simultaneous AIA 304 Å image, and the FOV is the same as that of the bottom row of Figure 1. (b-c) Unsigned positive and negative magnetic fluxes calculated in the areas indicated by the black circles and the white ovals in panels (a1-a8). The blue vertical lines mark the start time of F's eruption. (An animation of HMI LOS magnetograms is available. The animation lasts 27 seconds, has the same FOV as that of panels (a1)-(a8), and covers the time from 21:30 UT of March 21 to 05:29 UT of March 22. The cadence of the HMI magnetograms is 45s.)

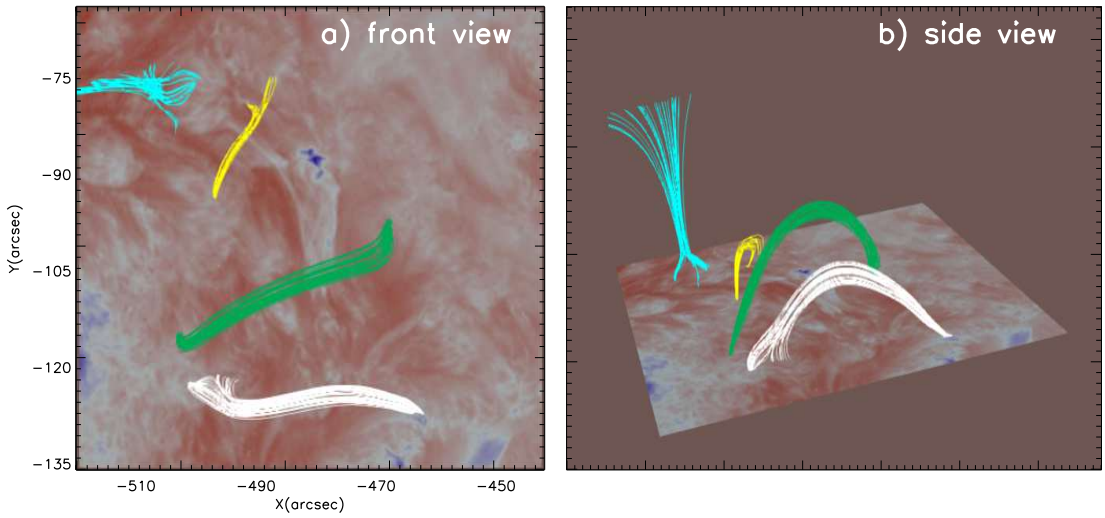

Figure 5. Coronal magnetic field obtained from the local potential field extrapolation explains the asymmetry of the two-sided loop jet. (a) Front view. (b) Side view. The background image is the 05:09:24 UT AIA 171 Å image, while the four groups of curves with different colors are the extrapolated 04:00:31 UT coronal magnetic field lines at some specific positions.